Journal of Hydrology: Regional Studies 23 (2019) 100602

Contents lists available at ScienceDirect

Journal of Hydrology: Regional Studies

journal homepage: www.elsevier.com/locate/ejrh

Mapping saltwater intrusion with an airborne electromagnetic method in the offshore coastal environment, Monterey Bay, California

Meredith Goebel[a,*], Rosemary Knight[a], Max Halkjær[b]

[a] Stanford University, Department of Geophysics, 397 Panama mall, Stanford, CA, 94305, United States
[b] Ramboll, Olof Palmes Allé 20, DK-8200 Aarhus N, Denmark

ARTICLE INFO

Keywords:
Saltwater intrusion
Coastal aquifer
Airborne electromagnetic (AEM)
Electrical resistivity tomography (ERT)
Offshore

ABSTRACT

Study Region: The northern coast of the Monterey Bay, California, USA, extending from the coastline to 3.5 km offshore.

Study Focus: Three-hundred and twenty line-kilometers of airborne electromagnetic (AEM) data were acquired offshore. These data spanned 20 km of coastline, extending up to 3.5 km offshore in water up to 18 m in depth. Inversion of these data resulted in resistivity models extending to depths between 50 and 200 m below sea level. The data were interpreted in conjunction with onshore monitoring well data, hydrologic and geologic reports, and electrical resistivity tomography (ERT) data to locate the freshwater/saltwater interfaces throughout the region. A resistivity-to-water-quality transform was established using well-based water quality and resistivity logging measurements. For resistivity values that could not be converted to water quality with this transform, local auxiliary information was used on a case-by-case basis to interpret the observed features. Some low resistivity anomalies were identified near the shore at depth, which were interpreted to be artifacts of the 1D assumption in the inversion scheme used for these AEM data.

New Hydrogeological Insights for this Region: We found that the acquisition of AEM data provided valuable information about water quality in the offshore extents of the aquifers, a region inaccessible to traditional monitoring methods, but one that plays an important role in the modeling, prediction, and management of saltwater intrusion.

1. Introduction

In coastal regions around the world, there is a dynamic interface between fresh groundwater and saline ocean water. The location and geometry of a freshwater/saltwater interface is dictated by density and pressure gradients within the adjacent water bodies, as well as all other hydrogeologic conditions that control subsurface flow. In many cases both natural and anthropogenic changes in hydrologic systems have resulted in the interface migrating inland, in a process called saltwater intrusion. Saltwater intrusion can have significant economic and ecological impacts (Johannes, 1980; Werner et al., 2013; Michael et al., 2017), and therefore is an important issue in coastal groundwater management. With ˜40% of the global population living within 100 km of the coast (CIESIN, 2012), management of coastal groundwater resources is a critical component of achieving global freshwater security. A critical step in the management of coastal groundwater resources is mapping and monitoring the distribution of salinity in the subsurface. This is

* Corresponding author.

https://doi.org/10.1016/j.ejrh.2019.100602
Received 31 January 2019; Accepted 19 March 2019
Available online 01 April 2019

typically accomplished using water quality measurements made in wells, but there has been increasing recognition of a need to supplement this method in areas with complicated hydrogeologic conditions, or where limited well coverage results in large uncertainty in understanding the extent of saltwater intrusion. A specific challenge that we address in this study is the need to map the locations of freshwater/saltwater interfaces in the offshore region in areas where modeling suggests the imminent threat of saltwater intrusion, but no sampling data are available. The focus of this study is to assess the use of an airborne geophysical method as a way to locate freshwater/saltwater interfaces in the offshore coastal environment.

In recent years geophysical methods of imaging the subsurface have been shown to be highly effective for large-scale exploration and characterization of the extent of saltwater intrusion in coastal environments. Two methods in particular that have proven successful are ground-based electrical resistivity tomography (ERT) and the airborne electromagnetic (AEM) method. These methods provide a measure of subsurface electrical resistivity, which is highly sensitive to changes in pore fluid salinity, and thus are ideally suited to this application. De Franco et al. (2009); Martínez et al. (2009); Zarroca et al. (2011); Pidlisecky et al. (2015); Goebel et al. (2017), and others have demonstrated the effectiveness of ERT for mapping saltwater intrusion onshore. Both time-domain and frequency-domain AEM methods have been demonstrated to be useful in imaging onshore saltwater intrusion, as shown by Fitterman and Deszcz-Pan (1998); Teatini et al. (2011); Gunnink et al. (2012); Jørgensen et al. (2012), and others. The AEM method has the advantage of being able to give extensive spatial coverage relatively rapidly, as well as sample areas difficult or impossible to access with other methods. One such area is the offshore coastal environment, where the use of monitoring wells is impractical given the high cost of installing underwater wells. The presence of the seawater has little logistical impact on the ability to collect AEM data, but there is concern about the impact of the seawater on the data themselves, as such a highly conductive feature at the surface could make it difficult to investigate the structures beneath it.

The capability of AEM data to image beneath shallow saltwater bodies in lagoon and offshore environments has been explored in recent studies (Kirkegaard et al., 2011; Pedersen et al., 2017). These have found that while there is the expected decrease in depth of investigation beneath the conductive seawater, and convergence during inversion of the data to obtain the resistivity model can be difficult, AEM data can still yield useful information for understanding conditions within the offshore extent of aquifers. Pedersen et al. (2017), for example, mapped a freshwater lens extending in the subsurface offshore, and were able to image to depths of over 80 m in ocean depths of 20 m off the coast of the Netherlands. These examples have been successful, but with a limited number of such studies, there is a need for further research in different hydrogeologic settings to better understand the utility of offshore AEM data for mapping and monitoring coastal groundwater resources.

This study was designed to explore the use of AEM data to image the subsurface region from the coastline to a distance of up to 3.5 km offshore along the northern coast of Monterey Bay, California. This is a region where all of the aquifers are currently experiencing, or are threatened by, saltwater intrusion. Three previous geophysical investigations successfully demonstrated the capability of electrical/electromagnetic imaging methods to help resolve the distribution of, and hydrogeologic controls on, saltwater intrusion in this region. Long offset ERT was used in two studies along the coast of Monterey Bay (Pidlisecky et al., 2015; Goebel et al., 2017), and AEM data were acquired in the Salinas Valley (Gottschalk et al., 2018). Along much of the northern coast of the bay, in the Soquel Creek area, ERT data in the Goebel et al. (2017) study were interpreted to show predominantly freshwater in the top 100 mbsl at the shoreline, consistent with measurements made in wells inland. In those areas where ERT and well data indicated that the aquifers were saturated with freshwater onshore, the critical question posed by local groundwater managers, and the motivation for this study: where are the freshwater/saltwater interfaces located within the various hydrogeologic units? They could be offshore and/or could be deeper than the screened intervals of the wells onshore.

The goal of this study was to locate the freshwater/saltwater interfaces in the Santa Cruz Mid-County region by complementing onshore well and ERT data with offshore AEM data; where the AEM data were used to map out the variation in water quality in the offshore extent of the groundwater aquifers. The findings presented here reveal the complex nature of saltwater intrusion in the region, and highlight the ability of the AEM method to image these complex features offshore, a region difficult to access with well-based monitoring methods. The findings also demonstrate some challenges of this method in coastal environments. While specific findings are unique to this study area, the insights gained contribute to the assessment of the AEM method for offshore coastal hydrogeologic investigations, and to the development of this method for investigating similar coastal systems elsewhere in the world.

2. Study area

The location of the study area, here referred to as the Soquel Creek area, is in the Monterey Bay region of California, and is shown in Fig. 1c and outlined in black in Fig. 1a and b. With limited surface water resources, the Monterey Bay region depends on groundwater to meet > 80% of its freshwater needs (California Water Foundation, 2014); during times of drought this percentage can increase. In the Monterey Bay region, extensive groundwater extraction has lead to significant saltwater intrusion within some of the actively pumped aquifer units, with saltwater water observed in monitoring wells more than 16 km inland at some points (Monterey County Water Resources Agency, 2014). While the Soquel Creek area has not experienced nearly as much saltwater intrusion as found in areas to the south, hydraulic head and water quality measurements suggest that saltwater intrusion is still a significant threat in this area (Hydrometrics, 2017). New legislation in the state of California specifically mandates that groundwater resources be managed so as to avoid 'significant and unreasonable' saltwater intrusion into aquifers (California Department of Water Resources, 2018). Characterizing water quality conditions in the offshore extent of aquifers is critical for fully understanding the hydrogeologic system, and planning management strategies to meet these new state requirements in the Soquel Creek area.

Fig. 1a shows the study area and surrounding Monterey Bay region with the location of the offshore AEM data acquired in May 2017; lines of data, shown in gray, were acquired parallel and perpendicular to the coastline, with the former so close together that

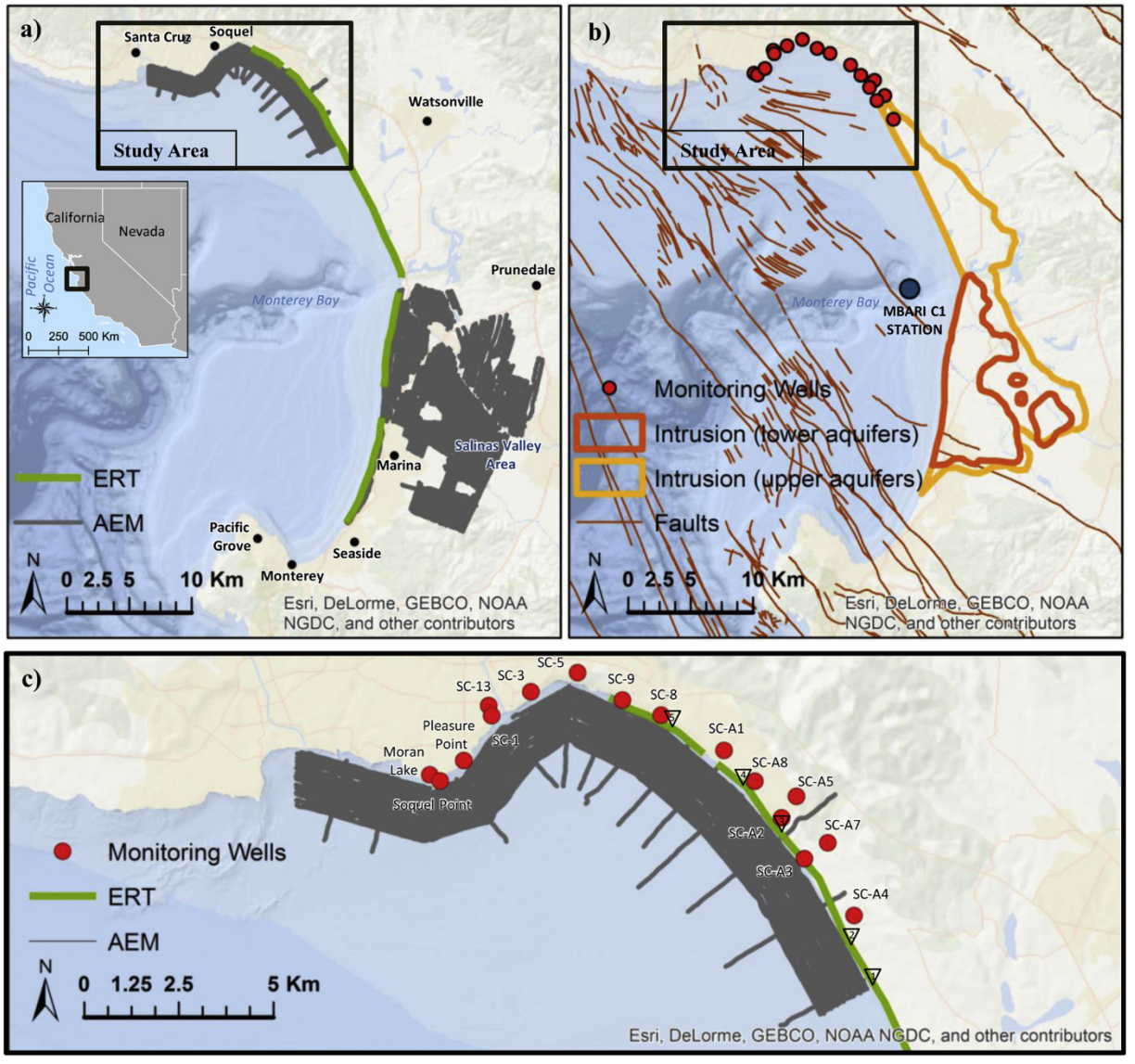

Fig. 1. Location of the study area within the greater Monterey Bay Region: a) showing locations of AEM data (in gray) for this study and in the Salinas Valley area from Gottschalk et al. (2018), ERT data from Goebel et al. (2017) in green, and the outline of the groundwater basins in the region in tan (DWR, 2017); b) showing locations of the monitoring wells closest to the coast within the study area in yellow, large rivers and streams in blue, faults in red, and the extent of saltwater intrusion in the upper aquifers in light orange, the extent of intrusion in the deeper 400 ft aquifer in dark orange, and the location of the Monterey Bay Aquarium marine monitoring station C1 in blue; c) showing a zoomed in view of just the study area showing the spatial relationship between the AEM data, ERT data, and monitoring wells discussed in the text, with names displayed next to the monitoring wells, and triangular markers along the ERT data marking points discussed in the text (For interpretation of the references to colour in this figure legend, the reader is referred to the web version of this article).

the separate lines are not visible in the figure. Three-hundred and twenty line km of data were acquired, along 20 km of the coastline, extending up to 3.5 km offshore in water up to 18 m in depth. This figure also shows the locations of other geophysical datasets within the region which will be discussed in this paper, including ERT, in green, spanning much of the coastline of the bay (Goebel et al., 2017) and onshore AEM data in the Salinas Valley area (Gottschalk et al., 2018) in gray, also collected in May 2017. Fig. 1b shows other key information for the interpretation and contextualization of these data. This includes the mapped extent of saltwater intrusion based on well water quality sampling (Monterey County Water Resources Agency, 2017; Pajaro Valley Water Management Agency, 2018). In the Salinas Valley area this mapped extent is divided into intrusion into the upper and lower aquifers, named the '180 ft' and '400 ft' aquifers, respectively, with the more inland boundary being that in the 180 ft Aquifer. It is important to note that these boundaries only show the extent of intrusion as reported by local agencies as interpolated spatial information. Some intrusion is known to exist near the coast in the north within our study area, but is not reported in a way that can be easily presented in this figure. Fig. 1b also shows a selection of the Soquel Creek monitoring wells closest to the coast within the study area, and the location

Table 1
Geologic formations, their properties, their hydrostratigraphic divisions within the Soquel Creek area, and the groundwater model designation (aquifer or aquitard) of each of the hydrostratigraphic units.

Geologic Formation	Properties	Hydrostratigraphic Units	Groundwater Model Designation
Aromas Formation	Poorly consolidated, medium to coarse sandstone with interbedded silt and clay	Aromas	Aquifer
Purisima Formation	Moderately consolidated, fine to medium sandstone with interbedded siltstone and claystone	DEF/F	Aquifer
		D	Aquitard
		BC	Aquifer
		B	Aquitard
		A	Aquifer
		AA	Aquifer
		Tu	Aquifer

of the Monterey Bay Aquarium Research Institute's marine monitoring station C1 (MBARI, 2018), a permanent monitoring location offshore where quarterly seawater chemistry measurements are made. Fig. 1c shows a zoomed in view of just the study area, showing the spatial relationship between the AEM data, ERT data, and monitoring wells discussed in this paper. Fig. 1c includes the names of the monitoring wells, as well as markers along the ERT line references in the interpretation of these data.

The geology of the study area consists of two primary water-bearing formations, the Aromas and the Purisima, underlain by a granitic basement. Descriptions of properties of these formations are found in column 2 of Table 1 (Department of Water Resources, 2003). Within the study area, the Purisima Formation can be further subdivided into a number of hydrostratigraphic units. These units are summarized from shallowest to deepest in column 3 of Table 1. The subdivision described in Table 1 is taken from the groundwater flow model of the region. Column 4 of Table 1 notes the designation (aquifer or aquitard) of each of these units in the groundwater model. Extensive discussion on the technical aspects of this model, including how the hydrostratigraphic boundaries were selected and what assumptions went into defining these units can be found in Hydrometrics (2015). We compare the new finding in this study to the hydrostratigraphic divisions in this model, as they are the boundaries that are used in the management of groundwater within the study area.

To visualize the hydrogeologic structures, views of the groundwater model hydrostratigraphy are shown in Fig. 2. In Fig. 2, the plan view shows which unit is closest to the surface. This model is extrapolated offshore, with the offshore region noted in partially transparent gray. Two cross sections, labeled A/A' and B/B' on the plan view, show the dip of these units.

The process of saltwater intrusion is sensitive to pumping, recharge, and hydrogeologic conditions. Within the Soquel Creek region there is significant spatial variation in each of these factors. As a result, this region is likely to have a complicated pattern of

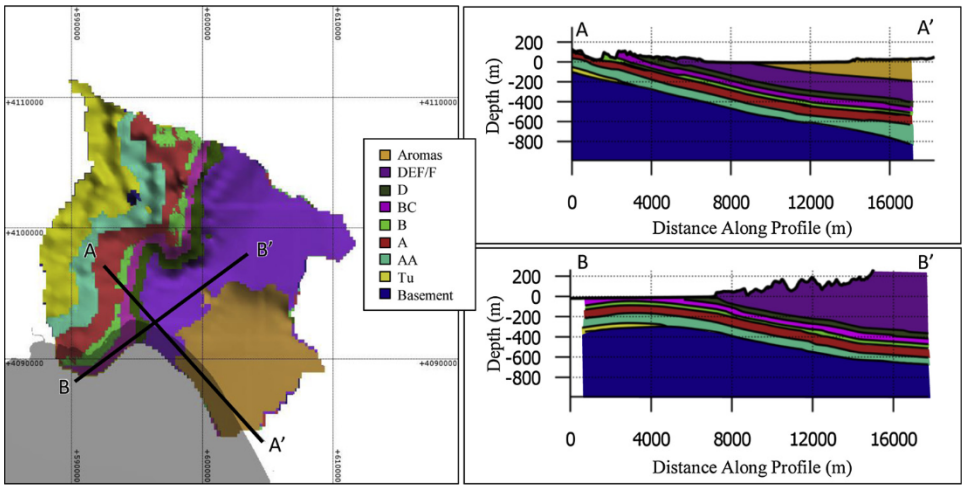

Fig. 2. Hydrostratigraphic boundaries of the groundwater model used for management of groundwater resources in the Soquel Creek Area, viewed in plan view on the left and along two cross sections on the right. The locations of the two cross sections are annotated as lines A/A' and B/B' on the plan view. In plan view, the areas in the figure offshore are marked in transparent gray.

intrusion, with the freshwater-saltwater interfaces located different distances from the coast in the different hydrostratigraphic units, or even within a single hydrostratigraphic unit. To date, onshore mapping of saltwater intrusion, using monitoring wells and coastal ERT data, shows a complicated distribution of fresh and saltwater in the subsurface. As shown in Fig. 1b, the coastal monitoring well network has detected intrusion into the upper aquifers in the southern portion of the study area but not the northern portion of the study area. Furthermore, within the portion of the study area where intrusion has been detected, well data suggest that the distance from the coast to which saltwater is found inland varies for the different upper aquifers. Further details on the spatial and temporal patterns of intrusion within this region can be found in Hydrometrics (2017). The critical issue motivating this study was the need to extend the mapping of the freshwater-saltwater interfaces offshore, where there is currently no data to constrain the locations of the freshwater/saltwater interfaces.

3. Materials and methods

3.1. AEM data acquisition, processing, and inversion

On May 23rd, 2017, 320 line kilometers of AEM data were acquired off the coast of the Soquel Creek area using the dual moment SkyTEM 304M system. This system utilizes hardware suspended beneath a helicopter, held ˜30 m above the ground surface. A forward modeling study as well as a ground-based time domain electromagnetic pilot study were used to determine the utility of an AEM survey in this region, and to design the best system configuration for an AEM acquisition in this setting. These studies motivated the use of an extremely low acquisition repetition frequency, allowing the system to collect data from 20 μs to very late time gates (20 + ms), maximizing the depths the system was sensitive to beneath the conductive seawater layer. During data acquisition, fifteen lines were flown parallel to the shore, with 100 m spacing between lines. These were connected with 12 tie lines perpendicular to the shore, spaced 1 to 2 km apart. Data acquisition was predominantly limited to the offshore region = for two reasons. The offshore was the area of greatest interest for understanding the locations of intrusion interfaces in the study area, and because much of the onshore portion of the study area consists of urban development, over which data acquisition is not permitted according to Federal Aviation Association regulations."

The data were both automatically and manually processed to remove noisy data. Minimal processing was required, as the conductive seawater and saturated sediments provided a large signal. Due to the high electromagnetic response from the conductive seawater and the sediments beneath the seafloor even the very late time gates showed signals well above the noise floor. Additionally, the majority of these data were acquired offshore, away from common noise sources such as power lines. This resulted in high quality data with a high signal to noise ratio.

Throughout this study we have employed the 1D form of AEM data inversion, an approach that assumes that the subsurface electrical resistivity varies with depth, but is laterally uniform. This assumption is generally considered appropriate as long as layers do not dip more than 30% (Auken, 2018). The spatial correlation between the data was taken into account using 3D spatial constraints on the 1D inversions. This approach is computationally efficient for large datasets, such as this one, and is well-suited to hydrologic applications. One limitation of this approach, however, is an inability to resolve sharp resistivity contrasts across vertical boundaries, where the 1D assumption is not valid. As shown in Heagy et al., (2018), 1D inversion of data in environments with abrupt lateral changes in resistivity can result in poor resolution of the true resistivity, and can introduce artifacts into the final resistivity models. Along the shoreline where freshwater extends offshore, resulting in sharp lateral changes in resistivity between the ocean and the freshwater-saturated sediments, we observed that the 1D model response had difficulties in fitting the actual measured data which created some model artifacts.

The data were inverted in Aarhus Workbench, using a 22-layer spatially-constrained inversion. Averaging of the data resulted in a 1D model of the variation in electrical resistivity with depth every ˜17 m along the flight lines. Model layer thickness starts at 0.8 m at the surface and increases with depth, with a final thickness of 40 m at 200 m depth, the maximum depth at which electrical resistivity values were determined. The thin layers at the surface were used to ensure that the thickness of the seawater, which ranges between 0 and 18 m thick along the offshore flight lines, could be modeled as accurately as possible while using a fixed layer thickness inversion. This was critical for the inversion of these data, as seawater is significantly more conductive than any other material expected to be present in this study area, and therefore should produce a large measured signal wherever it was present. It was not necessary to constrain the resistivity of the seawater layer within the inversion. The final inversion resulted in a data residual (a noise normalized RMSE between the measured and calculated data) of 0.545. This value is below 1, meaning that the data were fit within the noise level.

The depth of investigation (DOI) is defined as the depth to which models resulting from the inversion of geophysical data can be considered reliable. The DOI for each of the models was determined using the method outlined in Vest Christiansen and Auken, (2012). A universal cumulative sensitivity threshold of 0.1 was applied to determine the DOI; this is considered the 'standard' threshold in the Aarhus Workbench software. Using this threshold, the sensitive region of the dataset extends between 50 mbsl and 200 mbsl. The shallowest DOI occurs furthest offshore, where the conductive saline ocean water layer is the thickest, and the deepest DOI occurs onshore where there are thick packages of resistive material. The majority of these models have a DOI $<$ 100 mbsl, with the deepest offshore DOI being 165 mbsl. This was the spatial variation in DOI expected in this study area. The highly conductive seawater limits the ability to investigate features beneath the seafloor in the portions of the dataset that are the farthest offshore.

3.2. Resistivity-to-water-quality transform

In order to interpret the data collected to advance the understanding of the locations of the freshwater/saltwater interfaces within the study area, a transform between formation resistivity and pore water quality must be established. For the purposes of this paper we use the term water quality to qualitatively describe the salinity of the pore water within a saturated sediment ranging from freshwater to seawater. As reviewed in Knight and Endres (2005), the electrical resistivity of a sediment is a function of the resistivity of the solid phase of the sediment, and that of the contained pore water. Typically, most of the electrical conduction through a water-saturated sediment is through ionic conduction. As a result, the measured resistivity is highly sensitive to the volume of water-filled porosity and salinity, with increases in either resulting in a decrease in resistivity. The sediment type (lithology) has an influence on the electrical resistivity through the effect of porosity, but can also introduce another conduction mechanism; the surface conduction associated with clays results in a decrease in resistivity with an increase in clay content. Within the aquifers in Soquel Creek area, there is known to be significant variability in both lithology and pore water salinity. This makes establishing a transform from resistivity to water quality significantly more difficult than it would be if lithology could be assumed constant. Because of the unavoidable uncertainty introduced due to variable lithology, we adopted an approach whereby we defined two resistivity cutoffs: an upper formation resistivity value above which the sediments are interpreted to be freshwater saturated and a lower formation resistivity value below which sediments are interpreted to be saltwater saturated. The range of formation resistivity values between these cutoff values could not be easily transformed to water quality, as the values within this range could be the result of varying clay content, porosity, or water salinity. For resistivity values within this intermediate range, additional information is required for interpretation of water quality.

The cutoff values for this resistivity-to-water-quality transform were established using data from Soquel Creek Water District coastal monitoring wells, where we had measurements of electrical resistivity within the wells, in the form of resistivity logs, and measurements of water quality, given as total dissolved solids (TDS). The resistivity logs were acquired using wireline induction well logging tools, either by the Soquel Creek Water District when the wells were installed (Hydrometrics, 2012; Pueblo Water Resources, 2007), or in 2014 as part of the Goebel et al. (2017) study. The TDS measurements were taken from the TDS time series dataset collected and maintained as part of the Soquel Creek Water District and Santa Cruz Mid-County Groundwater Agency's coastal monitoring program (Hydrometrics, 2016). These TDS values are collected from the screened intervals within the agencies' dedicated coastal monitoring wells at least twice a year, and in some cases much more frequently. Because we needed data spanning the entire range of water quality conditions within the study area (freshwater saturated to saltwater saturated), we selected a subset of all the available monitoring wells, working with the ones that were closest to the coast presuming, that they were most likely to have water quality ranging from fresh to saline. From this subset we searched for wells with concurrent resistivity logs and TDS measurements. Only four nested well sets met these criteria (SC-A2, SC-A8, SC-8, and SC-9), with a total of 15 separate screened intervals between the four well sets. Three of these well sets had two different times for which approximately concurrent resistivity and TDS data were available. Schematics for each of these wells, showing the depths of screened intervals and the surrounding lithology are shown in Fig. 3. We sampled the resistivity logs within each of these screened intervals every 1.5 m, and paired each of those resistivity values with the TDS measurement for the screened interval. These measurements thus provide data pairs linking the resistivity of the saturated sediment to the TDS of the contained pore water, exactly what is needed to develop the relationship between resistivity measured with the AEM system and water quality. Some studies have shown that there can be challenges in comparing the absolute

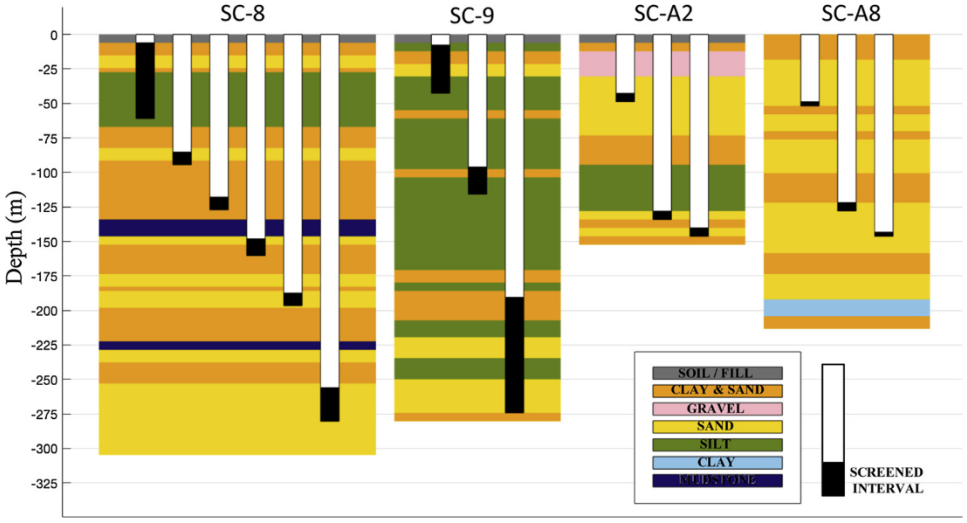

Fig. 3. Schematic of the four Soquel Creek nested monitoring well sets used for developing the resistivity-to-water-quality transform. The lithology for each well set, taken from the driller's lithologic log, is shown in color, overlain by each well in the nested set with the well's screened interval shown in black. Locations of these wells are noted in Fig. 1c.

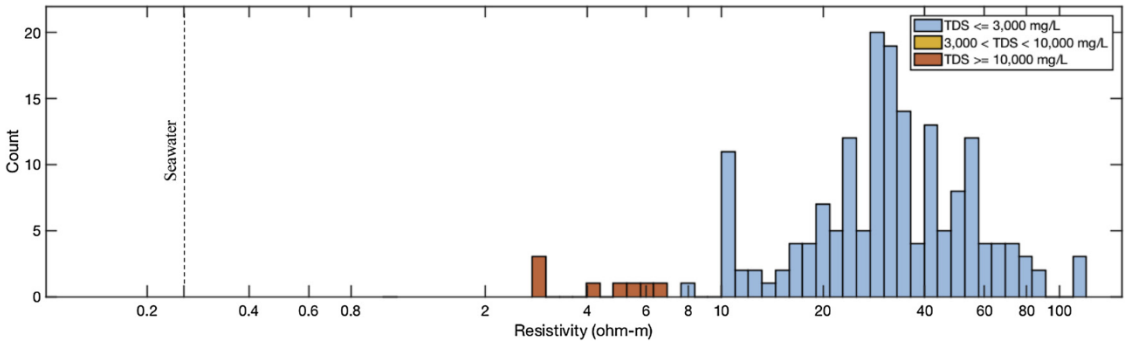

Fig. 4. Histograms of resistivity measurements sampled from the resistivity logs every 1.5 m within the screened intervals in Soquel Creek coastal monitoring wells, colored according the to TDS measurement made within that screened interval. The annual mean seawater resistivity taken from the MBARI C1 monitoring site is noted with a dashed line at 0.256 ohm-m.

resistivity values measured using surface geophysics and borehole geophysics due to inconsistent well calibration and/or difference in the sampled volumes of the two measurements. Analysis of the well logs in our study area indicates that they are high quality without any calibration issues. Comparison of collocated AEM data and borehole resistivity logs in the Salinas Valley area, where there were significantly more collocated monitoring wells and AEM measurements than in the Soquel AEM area, showed good agreement between the resistivity values determined with each method despite the different sampling volumes (Gottschalk et al., 2018).

The schematic in Fig. 3 illustrates one of the issues that complicated establishing the resistivity-to-water-quality transform. It can be seen that the screened intervals in these wells range from 6 m to 84 m in length, so can extend over more than one lithologic unit. It is possible that there is variation in pore water TDS between these lithologic units, and the TDS sampled in the screened interval is an average of that in each of these units. In compiling the data pairs, the resistivity values in multiple lithologic units were paired with the same single TDS value for that screened interval; this will increase the observed spread in the resistivity values for any given TDS value. The impact of this is that the established cutoff values will result in an under estimation of the volumes of the subsurface that are fully freshwater saturated and fully saltwater saturated.

The compilation of the data from the monitoring wells resulted in 180 resistivity/TDS data pairs. These pairs were then binned into three categories, with TDS intervals selected based on the potential utility of water for human use; TDS $>$ 10,000 mg/L (water of limited beneficial use), TDS 3,000–10,000 mg/L (water of potential beneficial use), TDS 0–3,000 mg/L (potential drinking water). These categories were taken from the State Water Resources Control Board (SWRCB) (2006), and the United States Environmental Protection Agency (US EPA) (1988).

Fig. 4 shows the histograms of these data. On this plot we have noted the annual mean seawater resistivity of 0.256 ohm-m measured at 10 m depth at the MBARI sampling station C1, the location shown in Fig. 1b (Monterey Bay Aquarium Research Institute, 2017). This value is consistent with global models of surface seawater resistivity (Tyler et al., 2017), as well as measurements made at other MBARI stations further offshore. This value is considered representative of the seawater resistivity at the time of AEM data acquisition, as time series of seawater resistivity in the bay show that temporal variability is minimal; monthly measurements in 2016 ranged between 0.244 and 0.26 ohm-m, and the largest anomaly in the monthly data since 1990 was a recorded resistivity of 0.23 ohm-m".

Fig. 4 shows there were many measurements in the 'water of beneficial use' category (TDS $<$ $=$ 3000 mg/L), very few at higher levels of TDS, with eight measurements in the 'water of limited beneficial use' category (TDS $>$ 10,000 mg/L), and no measurements in the 'water of potential beneficial use' category (TDS = 3,000–10,000 mg/L). This distribution is due to a sampling bias in these data, caused by the design of the nested well sets. The screened intervals of wells in these well sets were selected such that the deepest well's screened interval is below the depth where saltwater was encountered while drilling the borehole, and all subsequent shallower screened intervals were placed where the groundwater was still fresh. Because of this, there are only the eight measurements in the low resistivity range and no measurements in the intermediate range of resistivity values defined as the 'potential beneficial use' category (3000 mg/L $<$ TDS $<$ 10,000 mg/L).

Given the limited data set, the data from this study were combined with a similar dataset compiled from monitoring wells in the Salinas Valley area (Gottschalk et al., 2018). This region has suffered from significantly more intrusion than the Soquel Creek area, and water quality measurements made in wells here span a wide range of TDS values. Inclusion of these data helped mitigate the sampling bias in the Soquel Creek well data, as they cover a more complete range of the resistivity/TDS values expected to be imaged by the AEM data in the Soquel Creek area. In the Salinas Valley dataset, Gottschalk et al. discretized the resistivity logs into 15 cm intervals within the screened intervals, while the Soquel Creek resistivity logs were discretized into 1.5 m intervals. To account for this difference in discretization, when combining these datasets, the count in each resistivity bin from the Soquel Creek dataset was multiplied by a factor of 10. Fig. 5 shows the combined histograms for the data from monitoring wells in the Soquel Creek and Salinas Valley areas. This figure shows overlap in the three histograms between 3 and 30 ohm-m. If the entire area was composed of a single lithological unit, and we knew that the water quality measurements were from that unit alone, we would expect minimal overlap between the three histograms. In the cases of these data however, the variable lithology and large screened intervals (likely resulting

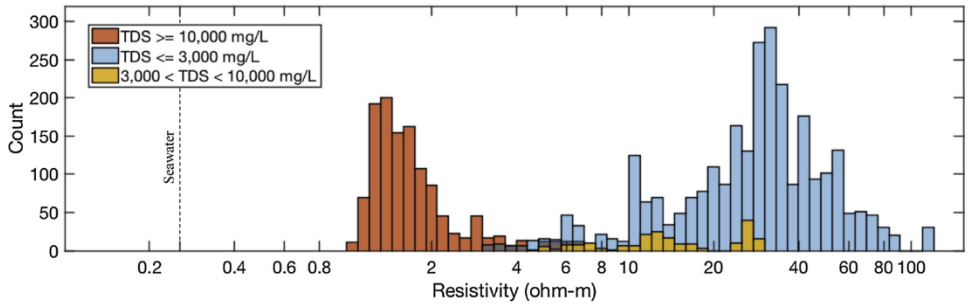

Fig. 5. Combined histograms of the well log resistivity measurements from the Soquel Creek and Salinas Valley regions, colored according the to TDS measurement made within the screened intervals matching the depths of the resistivity values. The annual mean seawater resistivity taken from the MBARI C1 monitoring site is noted with a dashed line at 0.256 ohm-m.

in water quality measurements of each interval which sampling more than one lithologic unit), there is significant overlap in these histograms.

Using these combined datasets two cutoff values were determined; all resistivity values < 3 ohm-m are considered to have TDS > 10,000 mg/L and are interpreted to be saltwater-saturated sediments or pure seawater, and all resistivity values > 20 ohm-m are considered to have TDS < 3000 mg/L and are interpreted to be freshwater-saturated sediments. While Fig. 5 clearly shows that it is possible to have freshwater-saturated sediments with resistivity values below 20 ohm-m, and saltwater-saturated sediments with resistivity values above 3 ohm-m, the intention of these cutoffs is to determine where we can identify, with confidence, the presence of fresh or saline water. There is a small group of resistivity measurements between 20 and 30 ohm-m in the 3,000–10,000 mg/L TDS range, but these are considered outliers. In this case, the isolated cluster of higher resistivity values can be traced back to a single shallow well in the Salinas Valley dataset. Looking at the resistivity log over the screened interval of this well, there is evidence that the water quality changes within this screened interval, despite this interval only having a single water quality measurement. As discussed previously, this would result in a wider spread in the possible resistivity values assigned to the TDS value in that screened interval. In this case we can say with confidence that the isolated cluster of higher resistivity values in the 3,000–10,000 mg/L TDS range have been assigned an inaccurate TDS value.

While the majority of the AEM data for this study were collected offshore, where sediments would be fully saturated, there are two tie lines that extend onshore where unsaturated material, above the water table, might be encountered. In the wells closest to the onshore tie lines, the depth to the water table ranges from 1 to 2 mbsl, with seasonal variations on the order of ~1 m (Hydrometrics, 2017). Because these regions will have high resistivity values that could be interpreted as freshwater saturated sediments using the cutoff established above, it is also important to also establish a cutoff value above which resistivity values would indicate that the subsurface is unsaturated. We adopted the cutoff value established by Gottschalk et al. (2018), who used a combination of well data and structure in the AEM data in the Salinas Valley area to select a value of 75 ohm-m, defining all resistivity values above this as indicating unsaturated sediments.

As an initial assessment of the AEM data, we produced a histogram of resistivity values, from the inversion of the AEM data, to display the relative volumes of the subsurface, sampled by the AEM data, corresponding to freshwater-saturated, saltwater-saturated, and unsaturated sediments. We sampled the resistivity models every meter above the DOI, regardless of model layer thickness; the resulting histogram is shown in Fig. 6. Using the defined cutoffs leads us to conclude that ~74.25% of the subsurface is saltwater-saturated sediments or pure seawater, 3.75% is freshwater-saturated sediments, 0.25% is unsaturated sediments, and 21.75% is sediments with water of an undetermined quality. The regions with undetermined water quality could be the result of a number of different water quality and lithology combinations, and thus will need to be interpreted using additional information, such as monitoring wells directly sampling the region, or the location of known hydrologic or geologic features. In this histogram there is a clear spike around the resistivity of seawater, measured as 0.256 ohm-m by the MBARI C1 marine station, resulting from the inverted resistivity models that include a seawater layer. We have not attempted to establish a cutoff between seawater and saltwater-saturated sediments in the values displayed in the histogram. This is because we have very few seawater resistivity measurements, and because we expect that the boundaries of the AEM resistivity model layers will not perfectly align, in all cases, with the location of the seafloor, as the thicknesses of model layers were fixed in the inversion of these data. If the seafloor exists within a model layer, the resulting resistivity of that layer will be influenced by both the resistivity of seawater and the resistivity of the underlying sediments.

3.3. Combined interpretation of ERT and AEM data

The Santa Cruz Mid-County Groundwater Agency AEM dataset was predated by another large geophysical survey, the collection of ERT data on the beach (Goebel et al., 2017). In this study, long offset ERT data were collected along 40 km of the beach in both a dipole-dipole array and gradient array, with electrodes spaced every 22.5 m along a 1.8 km active line length. These data were processed and inverted to produce resistivity profiles extending down to 280 mbsl, with absolute mean percent errors between 7.9 and 12.4%. Further discussion of the acquisition, processing, inversion, and interpretation of these data can be found in Goebel et al.

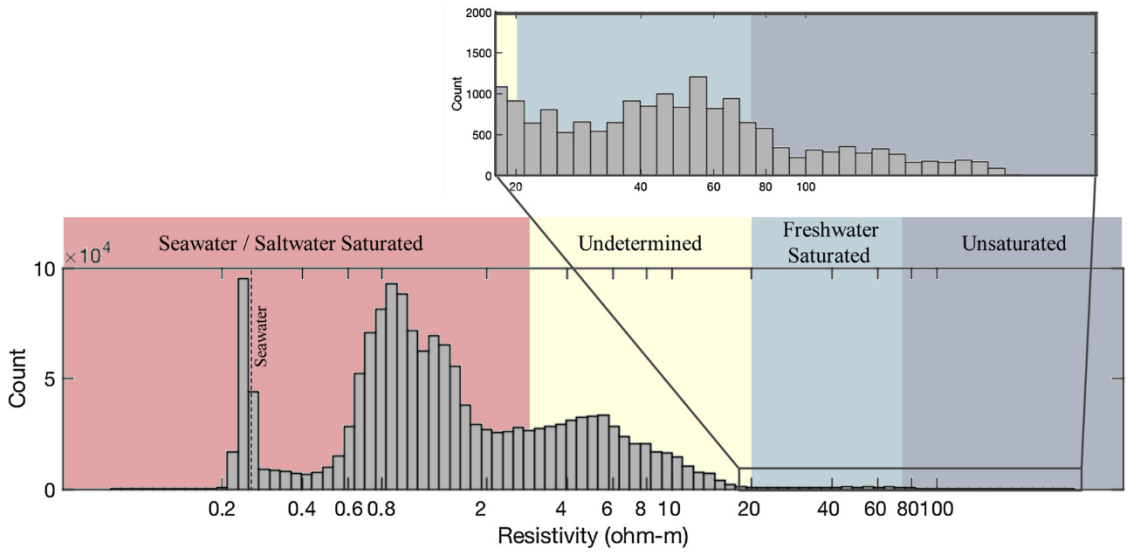

Fig. 6. A histogram of resistivity values resulting from the inversion of the AEM dataset, annotated with the water quality transform established using well data. The annual mean seawater resistivity taken from the MBARI C1 monitoring site is noted with a dashed line at 0.256 ohm-m. An enlarged view of the highest resistivity values is shown above the primary figure.

(2017).

In order to gain the most comprehensive understanding of water quality in the region, we wanted to use these onshore ERT data in the interpretation of the AEM data where the AEM data do not extend onshore in our study area. We were concerned, however, that there might be some difference in the data sets simply due to the difference in the physics of the measurements which can result in inconsistencies in the derived resistivity models from the two geophysical methods (Anschütz et al., 2015a,b). For this reason, we elected to first compare data from these two methods in the Salinas Valley area, south of our study area. Here, we had parallel lines of AEM and ERT data on average less than 50 m apart in an area where we knew, based on well data, that there was little change in water quality over the distance between these datasets. The ERT data in the Salinas Valley area were collected during the same acquisition, and using the same methodology, that gathered ERT data in the Soquel Creek region. The AEM data were collected in the Salinas Valley area within a month of the Soquel Creek AEM data, using the same SkyTEM system.

Fig. 7a–c show a comparison of the Salinas Valley AEM and ERT datasets, projected on a North-South oriented profile. In Fig. 7a we show the resistivity profile derived from the ERT data. The ERT data have been clipped at their DOI. A dashed line on top of the

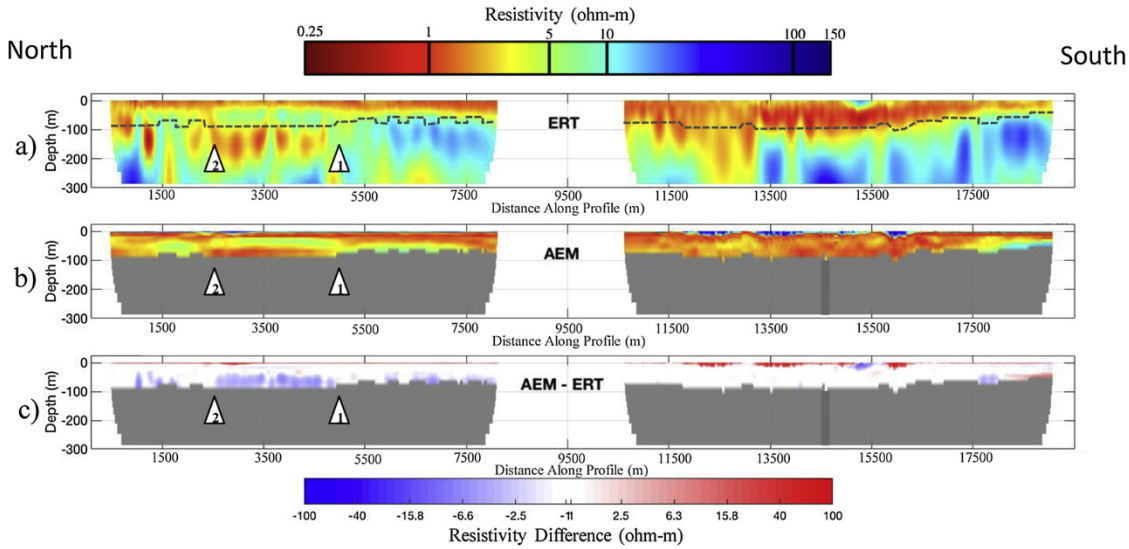

Fig. 7. Comparison of ERT and AEM datasets along the coast of the Salinas Valley area, with the ERT profile in 7a, nearest AEM data mapped onto the ERT profile in 7b, and the difference between the two (AEM-ERT) in 7c. The dashed line on the ERT profile represents the DOI of the AEM profile. Both AEM profile, and the difference profile are gray below the DOI of the AEM dataset.

ERT resistivity profile shows the DOI of the AEM dataset. In Fig. 7b we take the same 2D plane and show the corresponding resistivity profile derived from the AEM data by plotting the closest AEM-derived resistivity value for each point on the plane. We use the same color scale as the ERT profile, with gray indicating the region falling below the DOI in the AEM dataset. Fig. 7c shows the difference between the top two plots, created by subtracting the ERT resistivity values from the AEM values; we note that difference is plotted on a log scale for both positive and negative differences. The region below the DOI in the AEM dataset is again shown in gray.

Fig. 7 shows that overall both the resistivity values and large scale structures mapped with the two methods are very consistent. On the right hand side of the two plots we see very good agreement between the AEM and ERT profiles. On the far right of these profiles both show low resistivity in the upper 50 m with a transition to intermediate resistivity below 50 m. For the remainder of these two profiles, both have low resistivity values in the subsurface below 10 mbsl. On the left hand side of the two plots, both the AEM and ERT profiles have low resistivity values along much of the upper 30 m of the subsurface, with a transition to intermediate resistivity values below. The variable depth at which this transition occurs is consistent between the two profiles.

There is one difference between the two profiles, in the top ~10 m of the subsurface, that can be attributed to differences in the timing of data acquisition. The ERT data were acquired in October, following the dry season, while the AEM data were acquired in May, following one of the wettest winters on record. The red colors in the difference plot in Fig. 7c indicate that the AEM method finds much higher resistivity values than the ERT method. We conclude that this is due to the presence of significantly more freshwater in the near surface during the AEM data acquisition.

We see one difference between the two datasets that we attribute to the different forms of measurement, specifically related to resolution. We refer to the area between markers 1 and 2 in the depth range between 25 and 100 m. From drillers' lithologic logs and water quality data we know that within this zone the thick Salinas Valley Aquitard (a clay layer), lies above the saltwater-intruded 180 Ft Aquifer. In the AEM resistivity profile (Fig. 7b) these two layers are clearly visible, shown as the "green" clay layer overlying the "red" saltwater-intruded aquifer. In the ERT profile (Fig. 7a) however this whole package appears as a single unit with a resistivity value that falls between those of the two individual layers. This difference highlights the established ability of the AEM method to resolve small changes in resistivity on the low end of the resistivity spectrum (Lucius et al., 2006).

This comparison of the ERT and AEM datasets in the Salinas Valley area supports our use of the ERT and AEM data in the Soquel Creek area to assist in our interpretation of the variation in water quality in the distance between the two datasets. As seen in the comparison above, it is important to keep in mind the fact that changes in timing of the data acquisition can lead to changes in resistivity, particularly in the very near-surface, and that there can be differences in the resolution of the two methods.

4. Results and discussion

4.1. Presentation and interpretation of AEM inversion results

The models produced by inversion of the AEM data reveal complex, three-dimensional resistivity structures in the subsurface. We will interpret these structures using the resistivity-to-water-quality transform (established above), the beach ERT survey, data from onshore coastal monitoring wells and the MBARI marine station, the Santa Cruz Mid-County groundwater model (onshore and offshore), and the onshore and offshore Digital Elevation Model (DEM) (National Ocean and Atmospheric Association, 2012).

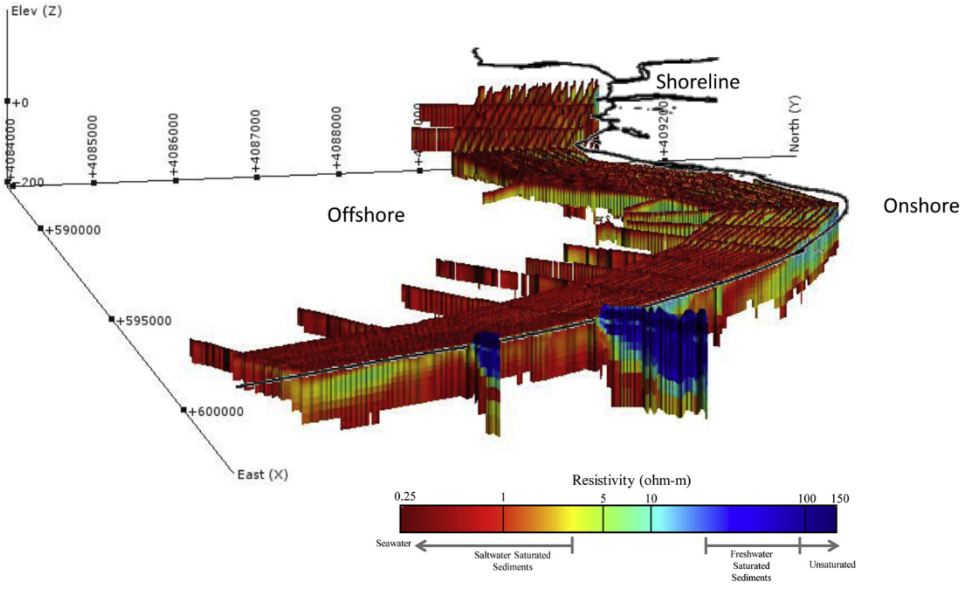

Fig. 8. Three-Dimensional view of the inverted resistivity models, for all values above 0.3 ohm-m (removes the seawater layer). Data are masked below the DOI. The shoreline, taken from where the DEM hit 0 mbsl, is marked with a black line.

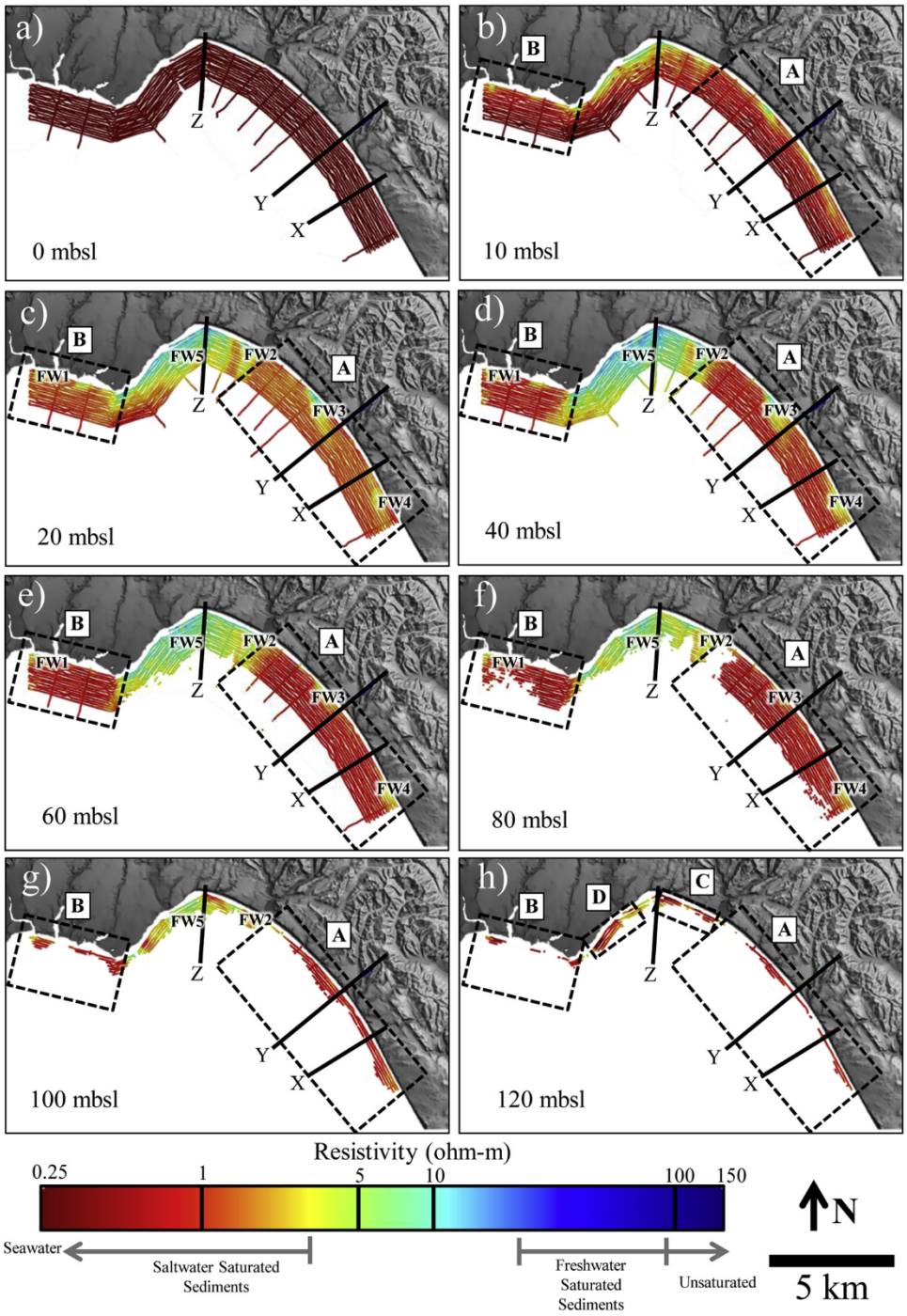

Fig. 9. Depth slices through the inverted resistivity models from 0 to 120 mbsl, next to the shaded DEM onshore. Data are masked below the DOI. Lines, boxes, and numbers on the figures indicate locations or regions that are discussed in the text.

Fig. 8 shows a 3D view of the inverted resistivity models from the AEM data. Models have been clipped at their DOIs. Resistivity values less than 0.3 ohm-m have been omitted, removing the seawater layer from this view, so as to better highlight the subsurface variability in resistivity. The shoreline, taken from where the DEM was equal to 0 mbls, is plotted in black. Color represents the resistivity values, spanning from 0.256 ohm-m, the annual mean resistivity of the near surface (< 10 m depth) seawater measured at the MBARI C1 marine station, to 150 ohm-m, the highest resistivity value found in this study. The color bar is also annotated with the cutoff values established in the '*Resistivity-to-Water-Quality*' section above. In discussing Fig. 9, and all subsequent figures, we describe the presence of "saltwater-saturated sediments" when the resistivity values are below the cut-off of 3 ohm-m, as shown in the color

bar, and “freshwater-saturated sediments” when the resistivity values are above the cut-off of 20 ohm-m, as shown in the color bar. We describe the other regions as being of “intermediate resistivity”, noting that these regions, depending on lithology, could have water of a quality ranging from saltwater to freshwater.

This figure shows that there is significant variability in resistivity, both laterally and with depth. They show that offshore there are portions of the subsurface that can be classified as freshwater-saturated as well as portions of the aquifer that can be classified as saltwater-saturated.

Fig. 9 a–h show plan views of the resistivity models derived through inversion of the AEM data, starting at sea level and extending down 120 mbsl. We show shaded DEM data in the adjacent onshore region. The interval between the depth slices start at 10 m, and then increases to 20 m after 40 mbsl. For spatial context, these data are overlain on a shaded relief image of the onshore DEM. The resistivity models are only shown above the DOI, which is the reason why the number of resistivity values (the extent of the models) decreases with depth. There are few locations where the DOI exceeded 120 mbsl. The figures are annotated with a number of markers that will be referred to in the following discussion.

An alternate way to view the data in Fig. 9 is with cross sections, which slice the dataset vertically, and allow for better visualization of the variation in the resistivity structure with depth. The AEM 1D models do not lie on a perfectly straight 2D plane. In order to make the cross sections we constructed a straight 2D plane coincident with as many of the AEM 1D models as possible. At locations where the AEM models do not lie exactly on this plane, the nearest models were plotted on the plane. The same procedure was followed in plotting data from nearby wells on the plane. The results are 2D cross sections plotting the AEM and well data. This plotting procedure resulted in a minor apparent mismatch between the DEM and the top of the models onshore in some of these figures, as the DEM was defined exactly of the 2D planes. All of the AEM models were less than 50 m from the 2D planes, and the subsurface geologic structures vary minimally over such a short distance, so this plotting approach this has no significant impact on our interpretation.

Fig. 10a–c show three such cross sections of the resistivity models perpendicular to the coastline, marked as lines X, Y, and Z in Fig. 9. These models are clipped at their DOIs. Also layered on Fig. 10 a–c are the DEM, hydrostratigraphic units from the groundwater model, nearby monitoring wells, and markers used in the discussion of these data. The locations of these cross sections were selected so that they sampled the areas where we see, in Fig. 9, relatively large-scale resistivity features.

Let us now refer to the plan sections and cross sections in Figs. 9 and 10 to interpret features seen within the AEM data with the goal of determining water quality in the offshore extent of the groundwater aquifers, and the locations of the freshwater/saltwater interfaces in the various hydrostratigraphic units along the coast.

One easy-to-interpret feature seen in the AEM dataset is the continuous low resistivity layer at the surface offshore, which corresponds to the seawater. This can be seen in the entire offshore region in Fig. 9a, and in the most distant offshore parts of Fig. 9b. The resistivity values in the seawater layer, consistently ~0.25 ohm-m, agree with the near surface (< 10 m depth) annual mean seawater resistivity value of 0.256 ohm-m measured at the MBARI sampling station C1. The consistency of the resistivity values in this layer across all the AEM models is evident in how narrow the peak around 0.25 ohm-m is in Fig. 6, compared to any other peaks in this figure. As can be seen in Fig. 10 a–c, the lower boundary of the seawater layer, as mapped by the AEM data, aligns very well with the mapped seafloor bathymetry. We find that the AEM method has accurately captured both the depth and resistivity of the seawater, providing evidence of the reliability of the method in this environment.

We now review the portions of the dataset where the AEM data indicate that the subsurface offshore is predominantly saltwater saturated. These areas were roughly grouped into the dashed Boxes A and B in Fig. 9. We will begin with a discussion of Box A, shown in plan view in Fig. 9 and in cross sections X and Y in Fig. 10a and b. Interpreting the AEM data in these figures using the resistivity-to-water-quality transform shown in the color bar, we conclude that most of the sediments offshore in Box A are saturated with saltwater. The two resistivity cross sections X and Y, in Fig. 10a and b, display the classic wedge shape associated with saltwater intrusion, with the depth at which saltwater-saturated sediments are found increasing inland with distance from the shore. We see a thick section of freshwater-saturated sediments in the upper portion of the onshore Aromas Formation, with evidence that saltwater extends onshore into the sediments within the lower portion of the formation. Both of the cross sections X and Y in Fig. 10a and b are overlain with the locations of the monitoring wells closest to the cross section, with the TDS values in their screened intervals annotated alongside the screened interval, and the distance between the well and the profile noted above the well. The TDS values in the Aromas Formation where the AEM data indicate freshwater-saturated sediments range from 145 to 364 mg/L, also indicating freshwater. The TDS value in the Aromas Formation where the AEM data indicate saltwater-saturated sediments is 18,000 mg/L, also showing saltwater within this formation. This agreement between the AEM and well data validates our approach to the interpretation of AEM data in terms of water quality. It also highlights the ability of the AEM data to fill in the spatial gaps in the monitoring well network, allowing us to track the freshwater/saltwater interface in the Aromas Formation away from the point locations where it is observed in wells.

In addition to showing saltwater-saturated sediments extending onshore in the Aromas Formation, Fig. 10b shows saltwater extending onshore in the deeper Purisima DEF/F unit (which is only above the DOI for a small number of the models shown in Fig. 10a). The two wells that are screened within this unit both show high TDS values, again agreeing with our interpretation of the AEM data. Here, the AEM data can be interpreted as showing saltwater extending at least 1.5 km inland within the DEF/F unit.

The AEM profiles parallel to the coastline within Box A in Fig. 9 show predominantly saltwater in the subsurface offshore. While this is useful in determining the water quality of the subsurface offshore, they do not allow us to locate the freshwater/saltwater interfaces within the hydrogeologic units imaged, as in most of Box A it appears the interfaces are inland of the closest AEM line parallel to the coast (~200 m offshore). Only the two tie lines discussed above, which extend onshore, are able to directly locate a freshwater/saltwater interface, and resolve its geometry as it extends from the shoreline onshore within the Aromas Formation. Next,

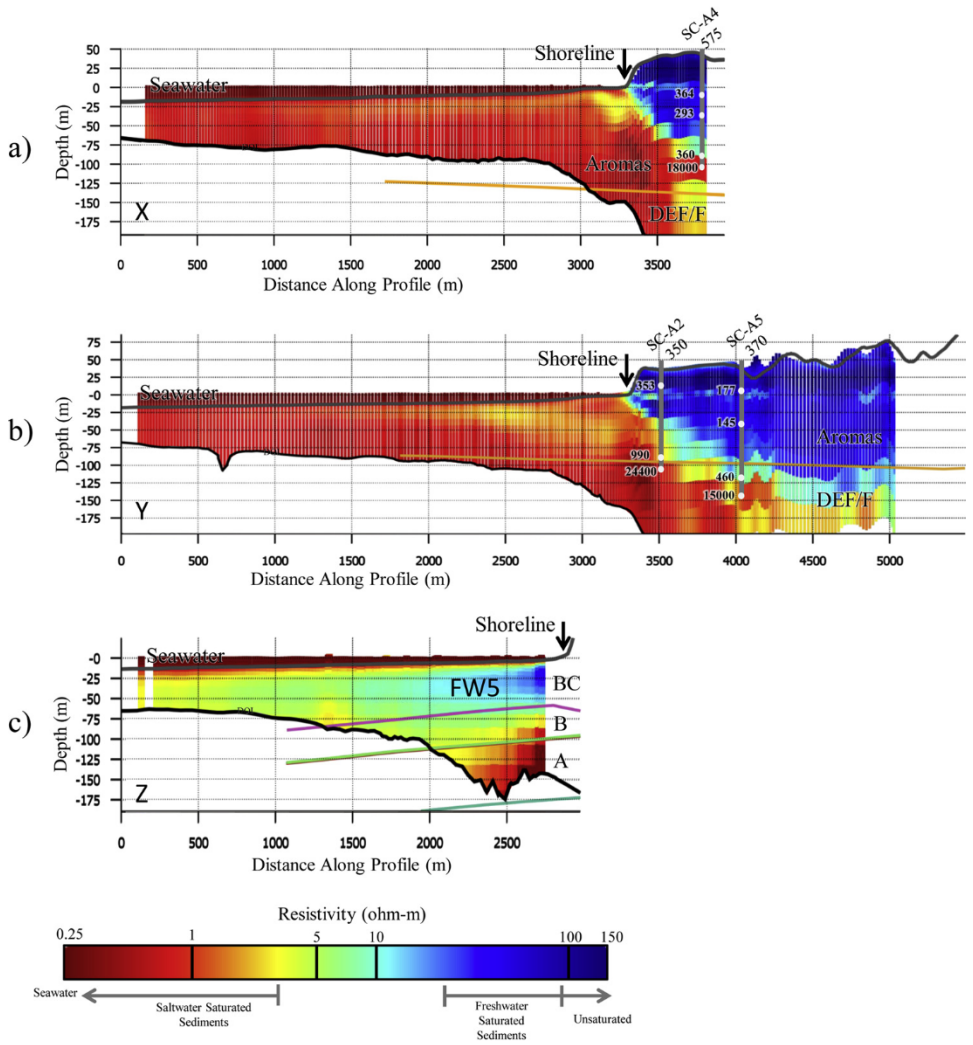

Fig. 10. Cross sections of the inverted resistivity models along the profiles 'X' (10a), 'Y' (10b), and 'Z' (10c) noted in Fig. 9. Data are masked below the DOI. Hydrostratigraphic boundaries from the groundwater flow model are noted with the same color scheme as in Fig. 9, and units are labeled according to the names given in Table 1. Monitoring wells are projected onto the cross sections, with the 2016 TDS values (in units of mg/l) measured in each of the screened intervals noted next to the depth of that screened interval. The onshore and offshore DEM are noted with a gray line.

we will use the combined interpretation of the closest AEM profile parallel to the shore and the long offset ERT profile along the beach. By including the ERT dataset in our interpretation of the AEM dataset, we can bridge the gap between the offshore AEM data and the onshore monitoring wells to better constrain the exact location of the freshwater/saltwater interface within each of the units imaged by the AEM dataset. This allows us to maximize the information gained from the new offshore dataset.

Fig. 11a and b show a comparison of the resistivity profiles created from inversion of the onshore ERT data, and the offshore AEM data along the closest flight line parallel to the coast, projected on a North-South profile. The distance between these two profiles is approximately 200 m. The ERT-derived resistivity profile is in Fig. 11a, and the AEM-derived resistivity profile is in Fig. 11b, both on the same color scale. Both profiles display results above their respective DOIs with the DOI of the AEM dataset shown as a dashed line on the ERT profile. In both figures, the two vertical dashed black lines mark the bounds of Box A seen in the plan views in Fig. 9. The two vertical dashed gray lines show where cross sections X and Y (seen in Fig. 10a and b, and located in plan view on Fig. 9) intersect these profiles. Included on both figures are the hydrostratigraphic units from the groundwater model (labeled as named in Table 1) and markers 1 to 5, which are referred to in the following discussion. For consistency, Fig. 11b is also annotated with the same 'FW' markers used in Figs. 9 and 10, referencing locations discussed later in the text.

A comparison of Fig. 11a and b shows that there are some locations where the two methods show similar resistivity values and structures in the subsurface, and some locations where they are quite different.

In the top few meters of the AEM profile is the low resistivity layer, corresponding to the seawater layer. This is not seen in the ERT profile as the data were acquired onshore.

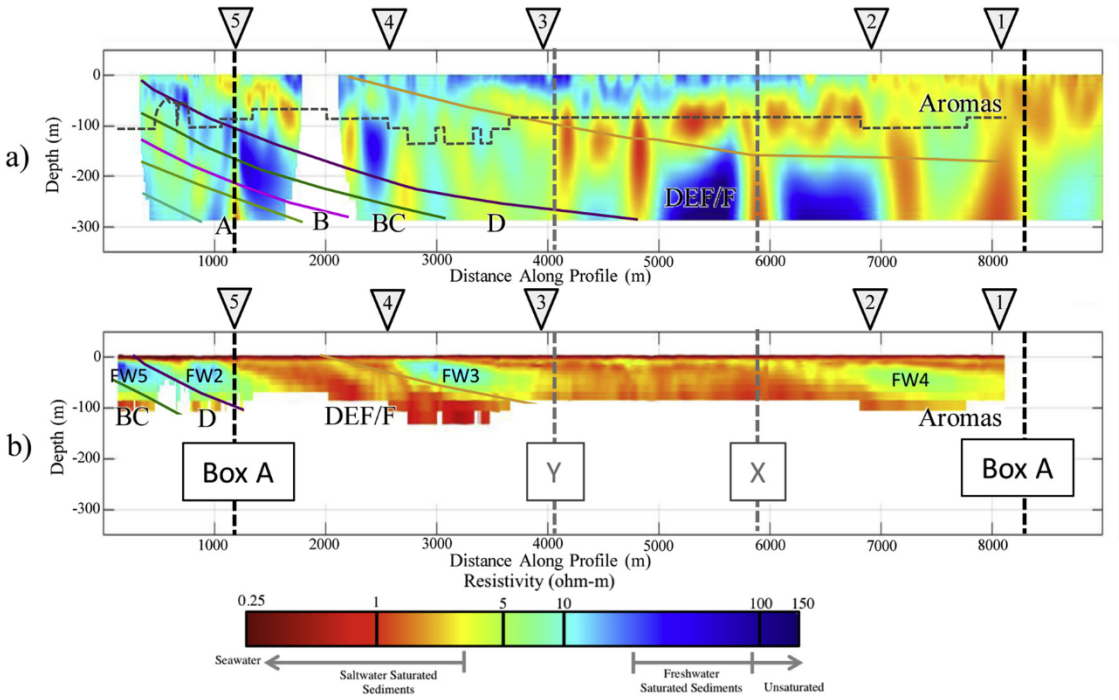

Fig. 11. Inverted resistivity from ERT data collected along the beach (a), and inverted resistivity from the closest offshore AEM flight line (b). The dashed gray lines mark the intersection of the cross sections shown in Figs. 10a and b with these two profiles, and the dashed black lines mark the boundaries of Box A in Fig. 9. Hydrostratigraphic unit boundaries are marked, and markers 1–5 at the top of the figures note locations referenced in the discussion of this figure. Markers 'FW2-5' reference locations discussed in the text.

Between markers 1 and 2, the two datasets show similar resistivity structures, suggesting that there is little change in the subsurface between these profiles. In the top ~25 m, both profiles predominantly show saltwater-saturated sediments (yellows through reds), though the AEM profile consistently shows lower resistivity values than the ERT profile, possibly suggesting more saline water offshore. Both then show a zone of intermediate resistivity (greens and yellows) beginning near the surface below marker 2, and extending to greater depths towards marker 1. This intermediate resistivity zone is much more defined in the AEM profile. A possible reason for this is that, as established in the '*Combined Interpretation of ERT and AEM Data*' section, the AEM method is better able to resolve small-scale changes in resistivity at the low resistivity end of the spectrum than the ERT method. Therefore, this intermediate resistivity unit, which has a resistivity only a few ohm-m higher than the surrounding saltwater-saturated sediments in the AEM profile, is much more clearly defined in the AEM profile. The fact that neither the ERT nor AEM profiles contain any resistivity values that fall in the zone classified as freshwater-saturated sediments, and a significant number of resistivity values that can be classified as saltwater-saturated sediments, suggest that the intrusion interface is inland of the ERT profile. This conclusion is consistent with water quality measurements made in monitoring wells. As shown in Fig. 1b, saltwater intrusion has been mapped onshore in the Aromas Formation using well data within this area.

Between markers 2 and 3 in Fig. 11 the two datasets are quite different. The AEM profile shows that the subsurface is almost entirely saltwater-saturated. The ERT profile shows saltwater-saturated sediments at depth, but in the upper 30+ m shows freshwater-saturated sediments or resistivity values in the intermediate range. This difference is interpreted to be the result of these datasets being collected on opposite sides of the freshwater/saltwater interface at the surface. The location of the ERT profile is such that it captures the transition from freshwater saturated to saltwater saturated sediments, whereas the AEM dataset is seaward of this transition at all depths. This interpretation is consistent with the data shown in Figs. 10a and b, where the saltwater-saturated sediments extended onshore in the classic wedge shape described by the Ghyben-Herzberg model, with a package of freshwater-saturated sediments above the intrusion front that increases in thickness moving onshore. While it fluctuates somewhat, the depth to the saltwater-saturated sediments in the ERT datasets is relatively constant between markers 2 and 3. Using the observed differences between the profiles in Fig. 11, and the understandings gained from the interpretations of Fig. 10a and b, we conclude that the saltwater-saturated sediments seen in the AEM data offshore connect to the saltwater-saturated sediments seen in the ERT data below 30 m, in a wedge shape, which extends a short distance onshore in the Aromas Formation.

Between markers 3 and 4 in Fig. 11b we see saltwater-saturated sediments at the top of the AEM profile, underlain by a region of intermediate resistivity, with more saltwater-saturated sediments at the base. The transition to saltwater-saturated sediments at the base of the layer of intermediate resistivity occurs along the boundary of the Aromas Formation and DEF/F units as mapped in the groundwater model of this region. In contrast, at the onshore location of the ERT profile, none of the subsurface is classified as saltwater saturated, with the high resistivity values corresponding to freshwater-saturated sediments in the top 30 m. We can use well

data, along with these two datasets, to develop an understanding of the location of the freshwater/saltwater interfaces in the Aromas Formation and the DEF/F unit.

Within the Aromas Formation, TDS measurements in well SC-A8 (˜275 m from the shore) indicate freshwater. Based on the well data and ERT profile, we can conclude that between markers 3 and 4 the freshwater/saltwater interface is likely entirely offshore in the Aromas Formation. The intermediate resistivity zone seen within the Aromas Formation in the AEM profile may represent a transition zone from freshwater to saltwater within this unit offshore.

Within the DEF/F unit, TDS measurements in well SC-A8 (˜275 m from the shore), indicate the subsurface is saltwater-saturated, while other monitoring wells further inland of this indicate the unit is freshwater saturated. Based on these well data, combined with the intermediate resistivity observed in the DEF/F unit in the ERT profile, and the saltwater-saturated sediments observed in the AEM profile, we conclude that the freshwater/saltwater interface exists onshore somewhere between SC-A8 and the surrounding monitoring wells to the north and west, within the DEF/F unit.

Between markers 4 and 5 the AEM profile shows the subsurface to be fully saltwater-saturated. The ERT profile shows freshwater-saturated sediments in the near surface, with patches of saltwater-saturated sediments in the DEF/F unit near marker 5. Within the Aromas Formation, we interpret the contrast between these two profiles as their being on opposite sides of the freshwater/saltwater interface, placing its location somewhere offshore, between the two profiles in Fig. 11. This interpretation is supported by TDS measurements in the nearest monitoring well, SC-A1, located ˜340 m inland from the shore, which indicate freshwater in the Aromas Formation.

Within the DEF/F unit, comparison of the ERT and AEM profiles suggests significant variation in the location of the freshwater/saltwater interface over a short distance. Near marker 5, we interpret the saltwater-saturated patches seen in the DEF/F unit in the ERT profile to be the onshore extent of the saltwater-saturated sediments in DEF/F unit seen in the AEM profile. This interpretation would suggest that near marker 5, the freshwater/saltwater interface is inland of the ERT profile. Contradicting this interpretation is a measurement of freshwater in monitoring well SC-8 located ˜100 m from the shore; but the long length of the screened interval of the well makes this measurement unreliable.

Near marker 4 in the DEF/F unit, the ERT profile shows freshwater-saturated sediments in the upper 50 m of the subsurface, while the AEM profile shows saltwater-saturated sediments everywhere. Here, we interpret the two profiles as being on opposite sides of the freshwater/saltwater interface, placing its location somewhere offshore, between the two profiles in Fig. 11. This is supported by measurements of freshwater in the DEF/F unit in SC-A8, the nearest well to marker 4. Our interpretation, placing the freshwater/saltwater interface onshore near marker 5, and offshore near marker 4 shows how variable the location of the interface can be within a single unit. The sharp boundary between these two zones, and the fact that this boundary appears to parallel the boundaries between the hydrostratigraphic units in Fig. 11b, suggests that the variation within this unit could be the result of further lithologic stratification within the unit.

With the joint interpretation of the AEM and ERT datasets, we have been able to better constrain the locations of the freshwater/saltwater interfaces within Box A, where the AEM data showed the subsurface was predominantly saltwater-saturated. Let us now consider Box B shown in Fig. 9, in the easternmost portion of the AEM dataset. In this region no AEM tie lines extend onshore, and there are no coastal ERT data. There are, however, a number of monitoring wells near the coast with water quality measurements that can be compared to the offshore AEM data.

As seen in Fig. 9, all of the regions sampled by the AEM data within Box B show the subsurface to be saltwater-saturated. Contrary to what is seen in the AEM dataset, the majority of the water quality measurements in wells inland of Box B suggest that onshore sediments are freshwater-saturated at all of the depths imaged by the AEM data. Only two of the monitoring wells show elevated TDS values. These are Soquel Point and Moran Lake monitoring wells, shown in Fig. 1b. These wells show TDS values of 2400 and 510 mg/L in 2016, respectively, within the A hydrostratigraphic unit (Hydrometrics, 2017). While these TDS values are below the limit for our 'saltwater-saturated' classification, they are higher than measurements made in wells further inland, within Box B. With the AEM data showing that just offshore the A unit is fully saltwater saturated, we conclude that these elevated TDS measurements represent the front of saltwater intrusion within this unit. These two same monitoring wells do not show evidence of intrusion in their deepest screened intervals, within the AA unit, despite the fact that the AEM data in Fig. 9 show that the subsurface is saltwater saturated offshore at all depths. A likely explanation for this is that differences in lithology and/or pumping rates between the two units is causing intrusion into the A unit before the AA unit. While the AEM data do not allow us to determine the exact location of the freshwater/saltwater interface within Box B in Fig. 9, they do constrain it to being within the ˜200 m between the wells at the shore, and the first AEM profile offshore, at all depths for most of Box B.

Referring again to Fig. 9, let us now discuss the areas offshore where the subsurface is either of intermediate resistivity (light green to mid-blue on the resistivity color scale), or resistive enough to be classified as freshwater saturated. These locations are annotated with 'FW1'-'FW5' in Fig. 9, and where they are present in Figs. 10 and 11. The largest of these, at noted by 'FW5' in Fig. 9, can be seen to extend as far as 2.5 km offshore, from the seafloor to the bottom of the DOI. As was discussed in the '*Resistivity-to-Water-Quality Transform*' section above, values within the intermediate resistivity range could represent a wide range of pore water salinities, depending on the lithology (specifically the clay content). For this reason, these features must be interpreted using auxiliary information.

Features 'FW1'-'FW4' are all located near the mouths of streams or rivers that connect to the ocean, some seasonally and some year round. Our interpretation is that these regions have higher water quality associated with these features due to recharge through the base of the streams or rivers, or subsurface stream flow. The feature labeled 'FW3' in Fig. 9, appears to be connected to the larger region of intermediate resistivity values in the ERT dataset, shown between markers 3 and 4 in Fig. 11, and to freshwater observed in monitoring wells onshore.

The larger feature labeled 'FW5' is also interpreted to correspond to a region of higher water quality. As with the features labeled 'FW1'-'FW4', this zone is connected to the mouths of a number of rivers and streams, which are likely introducing the fresher water to this area. A cross section through this feature can be seen in Fig. 10c. Within Fig. 10c, this intermediate resistivity feature is seen to fill all of the hydrostratigraphic BC unit. Closest to the shoreline in Fig. 10c, the resistivity values in the BC unit are high enough to be classified as freshwater-saturated sediments. The resistivity values in this unit then gradually decrease with increasing distance from the shore, in a transition from the freshwater-saturated region to the surrounding regions of fully saltwater-saturated sediments.

4.2. Assessment of anomalously low resistivity features

As discussed in the '*AEM Data Acquisition, Processing, and Inversion*' section, this study employed a 1D, spatially-constrained inversion scheme, which may not be appropriate for use where there are abrupt lateral changes is resistivity that violate the 1D assumption. There are two areas with zones of anomalously low resistivity values near the coast that we interpret to be artifacts of the inversion scheme due to such abrupt changes in resistivity. The locations of these features can be seen in Fig. 9h, within the dashed Boxes C and D. A cross sectional view through one of these features can be seen at the bottom of Fig. 10c near the shoreline. These features are above the DOI, and examination of the raw data and inversion results would not suggest that these are the result of any noise source. Despite this, there are a number of reasons to conclude that these features are not real. The first is that the standard deviations on the resistivity values with the layers containing the anomalous values are significantly higher than elsewhere in the models. The second was that there were challenges in reaching good inversion convergence on the data. Lastly, these are highly unlikely to be hydrogeologic features, for a number of reasons. These features do not appear to be connected to saltwater intruded sediments further offshore. Given the hydrogeologic setting and depositional history, any large low resistivity feature in a unit onshore would be expected to connect to saltwater saturated sediments in that same unit offshore. Additionally, the inverted resistivity values within these features are very low, in some cases lower than that of pure seawater (0.25 ohm-m), which cannot be explained.

4.3. Implications for groundwater management

The interpretation of the AEM data acquired in the offshore coastal environment, in combination with the existing understanding of this region from ERT data and monitoring wells, have a number of implications for groundwater management in this region. Some of the more important of these are summarized below.

One management strategy, in areas under threat of saltwater intrusion, is to ensure that groundwater elevations are maintained at or above the minimum level needed to prevent intrusion, as determined through groundwater modeling; this minimum level is referred to as the protective groundwater elevation. Interpretation of the AEM dataset within the regions enclosed by Box A and Box B of Fig. 9 suggests that it is critical to reach and/or maintain protective groundwater elevations in these regions. At present, the onshore sediments in these regions are predominantly saturated with freshwater, with limited evidence of saltwater saturation. But the AEM data have revealed that the freshwater/saltwater interface is very close to the coastline, with the subsurface predominantly saltwater saturated just offshore. Combining the interpretation of the AEM dataset with onshore well data suggest specific priority areas within the regions enclosed by Box A and Box B. One such area is the portion of the actively pumped DEF/F unit that falls in Box A, where a few onshore monitoring wells have encountered intrusion; a number of these wells show groundwater elevations below their protective elevations. Another area is the portion of the A unit within Box B, as water quality measurements in two wells onshore suggest intrusion may be occurring in this unit. Proactively increasing groundwater elevations in these areas, either by reducing pumping or with managed aquifer recharge, could prevent further onshore movement of the freshwater/saltwater interface.

Interpretation of the intermediate resistivity zones labeled 'FW1'-'FW5' in Fig. 9 suggests that these are zones with lower salinity water. Most of these zones are above the depths of the screened intervals of pumping wells, and therefore do not likely represent future potential water sources for human use. Identification of these lower salinity water zones offshore is still useful however, as they likely play an important role in maintaining pressure against saltwater intrusion into the deeper portions of the hydrogeologic units in which they reside.

Lastly, this new AEM dataset and derived interpretations provide a baseline for assessing changes in the hydrologic system using future. This could be accomplished using ground-based monitoring (such as new and existing monitoring wells) or future AEM acquisitions. Extensive calibration of the system used to acquire these AEM data means that the acquisition can be repeated in the future and be compared to this baseline to map changes in subsurface resistivity over time.

5. Conclusions

The goal of this study was to determine the locations of the freshwater/saltwater interfaces within the Soquel Creek region. Our approach was to use a combination of offshore AEM data, onshore ERT data, and onshore monitoring well data. We found that by using an extremely low acquisition repetition frequency, allowing the system to collect at very late time gates (20+ ms), the AEM was able to image to the depths of interest (the upper aquifers), beneath seawater depth of up to 18 m. We found that interpretation of the extent of intrusion onshore from the AEM data, using a resistivity to water quality transform developed using only well data, were consistent with the previously mapped extents of intrusion onshore.

Where a freshwater/saltwater interface was present where AEM data was acquired the AEM data alone accurately located the interface. Where a freshwater/saltwater interface was not below a flight line, the location of the interface could be constrained using

joint interpretation of the AEM data and existing onshore datasets. We found the location of the freshwater/saltwater interfaces to be extremely variable within the study area, both between the different hydrogeologic units, and within individual hydrogeologic units at different points along the coast. Notably, we located a region where freshwater extended offshore within the subsurface.

This study has highlighted the importance of careful interpretation of AEM data in the context of their hydrogeologic setting. In coastal regions, such as studied here, with active saltwater intrusion, there can be abrupt and extreme lateral changes in resistivity. In these cases the 1D assumption in the inversion scheme most commonly used is not valid, and can result in inversion artifacts.

We conclude, based on the results of our study, that AEM data can play an essential role in mapping and monitoring saltwater intrusion, a role that cannot be as easily or cost-effectively filled by any other existing technology: the ability to determine the variation in water quality in the offshore extents of aquifers. The acquisition of data, in the offshore coastal environment, allowed us to better constrain the locations of the freshwater/saltwater interfaces within the various hydrogeologic units and identify the regions most at risk for future intrusion. These findings can support the development of proactive strategies for groundwater management by establishing a baseline for water quality in the offshore extents of the aquifers, and by highlighting the locations where management actions should be targeted.

Acknowledgments

We would like to thank Ron Duncan from the Santa Cruz Mid-County Groundwater Agency, which funded the acquisition, processing, and initial interpretation of the AEM data. We would also like to thank Ahmad Behroozmand from Stanford University for his guidance with AEM data processing and inversion, Ian Gottschalk from Stanford University for access to data from the Salinas Valley area, Seequent Limited for access to the Leapfrog Geo software used in interpretation of these data, and the Monterey Bay Aquarium Research Institute for permissions to use their ocean monitoring data. Additional funding was provided by the S.D. Bechtel Jr. Foundation, through a gift to the Water in the West Program in the Stanford Woods Institute for the Environment. Lastly, we would like to thank two anonymous reviewers, whose insightful comments helped greatly improve this manuscript.

References

Anschütz, H., Pfaffhuber, A.A., Real, C., Domaas, U., Sture, B., 2015a. Combined airborne and ground geophysics as a first phase towards a landslide warning system. Österreichische Ingenieur Archit 160.

Anschütz, H., Bazin, S., Pfaffhuber, A., 2015b. Towards Using AEM for Sensitive Clay Mapping – A Case Study from Norway. https://doi.org/10.3997/2214-4609.201413863.

Auken, E., 2018. Personal Communication.

California Department of Water Resources, n.d. SGMA Groundwater Management [WWW Document]. URL https://www.water.ca.gov/Programs/Groundwater-Management/SGMA-Groundwater-Management (accessed 06.07.2018).

California Water Foundation, 2014. Groundwater Issues Along California's Central Coast.

Center for International Earth Science Information Network, C.-C.U. 2012. National Aggregates of Geospatial Data Collection: Population, Landscape, And Climate Estimates, Version 3 (PLACE III).

de Franco, R., Biella, G., Tosi, L., Teatini, P., Lozej, A., Chiozzotto, B., Giada, M., Rizzetto, F., Claude, C., Mayer, A., Bassan, V., Gasparetto-Stori, G., 2009. Monitoring the saltwater intrusion by time lapse electrical resistivity tomography: the Chioggia test site (Venice Lagoon, Italy). J. Appl. Geophys. 69, 117–130. https://doi.org/10.1016/j.jappgeo.2009.08.004.

Department of Water Resources, 2003. California's Groundwater, Bulletin 118 Update 2003.

Fitterman, D.V., Deszcz-Pan, M., 1998. Helicopter EM mapping of saltwater intrusion in Everglades National Park, Florida. Explor. Geophys. 29 (240). https://doi.org/10.1071/EG998240.

Goebel, M., Pidlisecky, A., Knight, R., 2017. Resistivity imaging reveals complex pattern of saltwater intrusion along Monterey coast. J. Hydrol. 551, 746–755. https://doi.org/10.1016/J.JHYDROL.2017.02.037.

Gottschalk, I., Knight, R., Asch, T., Abraham, J., Cannia, J., 2018. Interpretation of Hydrostratigraphy and Water Quality from AEM Data Collected in the Northern Salinas Valley, CA.

Gunnink, J.L., Bosch, J.H.A., Siemon, B., Roth, B., Auken, E., 2012. Hydrology and Earth System Sciences combining ground-based and airborne EM through Artificial Neural Networks for modelling glacial till under saline groundwater conditions. Hydrol. Earth Syst. Sci. Discuss. 16, 3061–3074. https://doi.org/10.5194/hess-16-3061-2012.

Heagy, L., Kang, S., Crockett, R., Oldenburg, D., 2018. Open source software for simulations and inversions of airborne electromagnetic data. International Workshop on Airborne Electromagnetics. Kolding, Denmark.

Hydrometrics, 2012. Monitoring Well Destruction, Replacement, and New Installations at Various Locations Soquel, Capitola, and Aptos, CA.

Hydrometrics, 2015. Techincal Memorandum: Soquel-Aptos Groundwater Flow Model: Subsurface Model Construction.

Hydrometrics, 2016. Quarterly Report for Coastal Monitoring Data through October 2015.

Hydrometrics, 2017. Santa Cruz Mid-County Basin Groundwater Management Biennial Review and Report Water Years 2015–2016.

Jørgensen, F., Scheer, W., Thomsen, S., Sonnenborg, T.O., Hinsby, K., Wiederhold, H., Schamper, C., Burschil, T., Roth, B., Kirsch, R., Auken, E., 2012. Transboundary geophysical mapping of geological elements and salinity distribution critical for the assessment of future sea water intrusion in response to sea level rise. Hydrol. Earth Syst. Sci. 16, 1845–1862. https://doi.org/10.5194/hess-16-1845-2012.

Johannes, R., 1980. The ecological significance of the submarine discharge of groundwater. Mar. Ecol. Prog. Ser. 3, 365–373. https://doi.org/10.3354/meps003365.

Kirkegaard, C., Sonnenborg, T.O., Auken, E., Jørgensen, F., 2011. Salinity distribution in heterogeneous coastal aquifers mapped by airborne electromagnetics. Vadose Zone J. 10, 125. https://doi.org/10.2136/vzj2010.0038.

Knight, R., Endres, A., 2005. An Introduction to Rock Physics Principles for Near-Surface Geophysics, in: Near-Surface Geophysics. Society of Exploration Geophysics. Tulsa 31–70.

Lucius, J.E., Langer, W.H., Ellefsen, K.J., 2006. An Introduction to Using Surface Geophysics to Characterize Sand and Gravel Deposits.

Martínez, J., Benavente, J., García-Aróstegui, J.L., Hidalgo, M.C., Rey, J., 2009. Contribution of electrical resistivity tomography to the study of detrital aquifers affected by seawater intrusion–extrusion effects: the river Vélez delta (Vélez-Málaga, southern Spain). Eng. Geol. 108, 161–168. https://doi.org/10.1016/j.enggeo.2009.07.004.

Monterey Bay Aquarium Research Institute, n.d. No TitleData Repository [WWW Document].

Michael, H.A., Post, V.E.A., Wilson, A.M., Werner, A.D., 2017. Science, society, and the coastal groundwater squeeze. Water Resour. Res. 53, 2610–2617. https://doi.org/10.1002/2017WR020851.

Monterey Bay Aquarium Research Institute, 2017. Monterey Bay Time Series Data, Summary Reports [WWW Document]. (accessed 7.16.18). https://www.mbari.

org/products/data-repository/mbts_data/.
Monterey County Water Resources Agency, 2014. Historic Seawater Intrusion Map.
National Ocean and Atmospheric Association, 2012. Monterey, California 1/3 Arc-second MHW Coastal Digital Elevation Model.
Pajaro Valley Water Management Agency, 2018. Maps [WWW Document].
Pedersen, J.B., Schaars, F.W., Christiansen, A.V., Foged, N., Schamper, C., Rolf, H., Auken, E., 2017. Mapping the fresh-saltwater interface in the coastal zone using high-resolution airborne electromagnetics.
Pidlisecky, A., Moran, T., Hansen, B., Knight, R., 2015. Electrical Resistivity Imaging of Seawater Intrusion into the Monterey Bay Aquifer System. Groundwaterhttps://doi.org/10.1111/gwat.12351.
Pueblo Water Resources, 2007. Dolphin/Sumner Monitoring Well Project, Well Completion Report.
State Water Resources Control Board, 2006. Resolution No. 88–63 (as revised by Resolution No. 2006-0008): Adoption of Policy Entitled 'Sources Of Drinking Water'.
Teatini, P., Tosi, L., Viezzoli, A., Baradello, L., Zecchin, M., Silvestri, S., 2011. Understanding the hydrogeology of the Venice Lagoon subsurface with airborne electromagnetics. J. Hydrol. 411, 342–354. https://doi.org/10.1016/J.JHYDROL.2011.10.017.
Tyler, R.H., Boyer, T.P., Minami, T., Zweng, M.M., Reagan, J.R., 2017. Electrical conductivity of the global ocean. Earth Planets Space 69, 156. https://doi.org/10.1186/s40623-017-0739-7.
United States Environmental Protection Agency, 1988. Guidelines for Ground-Water Classification Under the EPA Ground-Water Protection Strategy.
Vest Christiansen, A., Auken, E., 2012. A global measure for depth of investigation. Geophysics 77, WB171–WB177. https://doi.org/10.1190/geo2011-0393.1.
Werner, A.D., Bakker, M., Post, V.Ea., Vandenbohede, A., Lu, C., Ataie-Ashtiani, B., Simmons, C.T., Barry, D.a., 2013. Seawater intrusion processes, investigation and management: recent advances and future challenges. Adv. Water Resour. 51, 3–26. https://doi.org/10.1016/j.advwatres.2012.03.004.
Zarroca, M., Bach, J., Linares, R., Pellicer, X.M., 2011. Electrical methods (VES and ERT) for identifying, mapping and monitoring different saline domains in a coastal plain region (Alt Empordà, Northern Spain). J. Hydrol. 409, 407–422. https://doi.org/10.1016/j.jhydrol.2011.08.052.